The Astrophysical Journal, 767:153 (10pp), 2013 April 20 doi:10.1088/0004-637X/767/2/153

THE NATURE OF FILAMENTARY COLD GAS IN THE CORE OF THE VIRGO CLUSTER

N. Werner[1], J. B. R. Oonk[2], R. E. A. Canning[1], S. W. Allen[1,3], A. Simionescu[1], J. Kos[2,4], R. J. van Weeren[5], A. C. Edge[6], A. C. Fabian[7], A. von der Linden[1], P. E. J. Nulsen[5], C. S. Reynolds[8], and M. Ruszkowski[9,10]
[1] Kavli Institute for Particle Astrophysics and Cosmology, Stanford University, 452 Lomita Mall, Stanford, CA 94305-4085, USA; norbertw@stanford.edu
[2] ASTRON, Netherlands Institute for Radio Astronomy, P.O. Box 2, 7990 AA Dwingeloo, The Netherlands
[3] SLAC National Accelerator Laboratory, 2575 Sand Hill Road, Menlo Park, CA 94025, USA
[4] Faculty of Mathematics and Physics, University of Ljubljana, Jadranska 19, 1000 Ljubljana, Slovenia
[5] Harvard-Smithsonian Center for Astrophysics, 60 Garden Street, Cambridge, MA 02138, USA
[6] Institute for Computational Cosmology, Department of Physics, Durham University, Durham DH1 3LE, UK
[7] Institute of Astronomy, Madingley Road, Cambridge CB3 0HA, UK
[8] Department of Astronomy and the Maryland Astronomy Center for Theory and Computation, University of Maryland, College Park, MD 20742, USA
[9] Department of Astronomy, University of Michigan, 500 Church Street, Ann Arbor, MI 48109, USA
[10] Michigan Center for Theoretical Physics, 3444 Randall Lab, 450 Church Street, Ann Arbor, MI 48109, USA
Received 2012 November 27; accepted 2013 February 26; published 2013 April 8

ABSTRACT

We present a multi-wavelength study of the emission-line nebulae located ∼38″ (3 kpc in projection) southeast of the nucleus of M87, the central dominant galaxy of the Virgo Cluster. We report the detection of far-infrared (FIR) [C II] line emission at 158 μm from the nebulae using observations made with the *Herschel* Photodetector Array Camera and Spectrometer (PACS). The infrared line emission is extended and co-spatial with optical Hα+ [N II], far-ultraviolet C IV lines, and soft X-ray emission. The filamentary nebulae evidently contain multi-phase material spanning a temperature range of at least five orders of magnitude, from ∼100 K to ∼10^7 K. This material has most likely been uplifted by the active galactic nucleus from the center of M87. The thermal pressure of the 10^4 K phase appears to be significantly lower than that of the surrounding hot intracluster medium (ICM), indicating the presence of additional turbulent and magnetic pressure in the filaments. If the turbulence in the filaments is subsonic then the magnetic field strength required to balance the pressure of the surrounding ICM is $B \sim 30$–70 μG. The spectral properties of the soft X-ray emission from the filaments indicate that it is due to thermal plasma with $kT \sim 0.5$–1 keV, which is cooling by mixing with the cold gas and/or radiatively. Charge exchange can be ruled out as a significant source of soft X-rays. Both cooling and mixing scenarios predict gas with a range of temperatures. This is at first glance inconsistent with the apparent lack of X-ray emitting gas with $kT < 0.5$ keV. However, we show that the missing very soft X-ray emission could be absorbed by the cold gas in the filaments with an integrated hydrogen column density of $N_{\rm H} \sim 1.6 \times 10^{21}$ cm^{-2}, providing a natural explanation for the apparent temperature floor to the X-ray emission at $kT \sim 0.5$ keV. The FIR through ultraviolet line emission is most likely primarily powered by the ICM particles penetrating the cold gas following a shearing induced mixing process. An additional source of energy may, in principle, be provided by X-ray photoionization from cooling X-ray emitting plasma. The relatively small line ratio of [O I]/[C II] < 7.2 indicates a large optical depth in the FIR lines. The large optical depth in the FIR lines and the intrinsic absorption inferred from the X-ray and optical data imply significant reservoirs of cold atomic and molecular gas distributed in filaments with small volume filling fraction, but large area covering factor.

Key words: galaxies: clusters: intracluster medium – galaxies: individual (M87) – infrared: ISM

Online-only material: color figures

1. INTRODUCTION

Massive giant elliptical galaxies in the centers of clusters with central cooling times shorter than the Hubble time frequently display spectacular optical emission-line nebulae (e.g., Johnstone et al. 1987; Heckman et al. 1989; Donahue et al. 1992; Crawford et al. 1999; McDonald et al. 2010). Associated cold molecular gas has also been detected in many of these systems, from near-infrared (NIR) K-band H_2 line emission (e.g., Jaffe & Bremer 1997; Falcke et al. 1998; Donahue et al. 2000; Hatch et al. 2005; Jaffe et al. 2005; Johnstone et al. 2007; Oonk et al. 2010) and CO observations (e.g., Edge 2001; Edge & Frayer 2003; Salomé & Combes 2003; McDonald et al. 2012). While the NIR spectra show H_2 line ratios characteristic of collisionally excited 1000–2000 K molecular gas, the CO emission traces the coldest (<50 K) molecular gas phases. Optical Hα+[N II] line emission arises from a thin ionized skin of 10^4 K gas on underlying reservoirs of cold neutral and molecular gas. CO observations indicate that the amounts of molecular gas in cluster cores can be large (Edge 2001), e.g., the cold gas mass in the center of the Perseus Cluster is approaching 10^{11} $M_\odot$ (Salomé et al. 2006, 2008, 2011). The observed level of star formation in these systems is, however, typically relatively small (e.g., O'Dea et al. 2008). Despite significant efforts to understand the origin and the excitation mechanism of these nebulae, their nature, energy source, and detailed physics remain poorly understood.

The relatively nearby ($d \sim 16.7$ Mpc; Blakeslee et al. 2009) giant elliptical galaxy M87 (NGC 4486), at the center of the Virgo Cluster, harbors a well-known extended optical Hα+[N II] filament system (Ford & Butcher 1979; Sparks et al. 1993). The proximity of this system allows us to study the physics of the emission-line nebulae in greater detail than is possible elsewhere. The Hα+[N II] nebulae in M87 were found to spatially coincide with filamentary soft X-ray emission

Table 1
Summary of Observations and of the Properties of the FIR Lines Integrated Over the Full 5 × 5 spaxel (47″ × 47″) Field of View of *Herschel* PACS

Line	Rest Frame λ (μm)	Observation Duration (s)	Line Flux (10^{-14} erg s^{-1} cm^{-2})	Instrumental FWHM (km s^{-1})	Observed FWHM (km s^{-1})	Line Shift (km s^{-1})
C II	157.7	3000	5.13 ± 0.5	240	361 ± 27	-62 ± 11
O I	63.2	3312	<36.7[a]	85	...	...
O IB	145.5	4480	<2.9[a]	255	...	...

Note. [a] 2σ upper limits.

(Young et al. 2002; Sparks et al. 2004), which can be modeled as ∼0.5 keV plasma in collisional ionization equilibrium (Werner et al. 2010). The emission-line nebulae also spatially coincide with C IV line emission at far-ultraviolet (FUV) wavelengths, which typically arises in gas at temperature $\sim 10^5$ K (Sparks et al. 2009, 2012). C IV line emission has so far not been detected in extended filaments in any other central cluster galaxy. Werner et al. (2010) showed that all of the bright Hα and UV filaments in M87 are found in the downstream region of a <3 Myr old shock front revealed by X-ray observations with *Chandra* (Million et al. 2010). This argues that the generation of Hα, UV, and soft X-ray emission in M87 is coupled to shocks in the hot X-ray emitting plasma. Based on these observations Werner et al. (2010) proposed that shocks induce shearing around the cooler, denser gas filaments, which promotes mixing with the ambient hot intracluster medium (ICM) via instabilities. By enhancing the rate at which hot thermal particles come into contact with the colder gas phases, mixing can in principle supply the power and the ionizing particles needed to explain the NIR to FUV line emission (Ferland et al. 2008, 2009; Fabian et al. 2011).

The launch of the *Herschel Space Observatory*, with its unprecedented sensitivity to far-infrared (FIR) line emission (Pilbratt et al. 2010), has opened new opportunities to study the coldest gas phases in galaxies. *Herschel* has enabled the first detections of atomic cooling lines of [C II], [O I], and [N II] in the X-ray bright cores of A1068, A2597 (Edge et al. 2010), and the Centaurus and Perseus clusters (Mittal et al. 2011, 2012). These lines are the dominant cooling lines for neutral interstellar gas and can be used as diagnostics to infer temperatures, densities, and radiation fields (e.g., Kaufman et al. 1999). Because carbon is the fourth most abundant element in the universe and has a low ionization potential, the 158 μm [C II] line is the most ubiquitous and best-studied (e.g., Malhotra et al. 1997, 2001). It is a tracer of gas with a temperature of ∼100 K.

To study the cold gas phases associated with the filamentary line emission nebulae in M87 we observed the regions of brightest Hα+[N II] filaments, extending to the southeast of the nucleus of the galaxy, with the *Herschel* Photodetector Array Camera and Spectrometer (PACS) at the wavelengths of [C II]λ157 μm, [O I]λ63 μm, and [O IB]λ145 μm. Here we report the results of these observations, as well as a reanalysis of deep *Chandra* X-ray data, *Hubble Space Telescope* (*HST*) optical and UV data, and long slit spectra obtained with the William Herschel Telescope (WHT). Section 2 describes the observations, data reduction, and analysis of the *Herschel* PACS, *HST*, *Chandra*, and WHT data. In Section 3, we summarize the results, and in Section 4 discuss the implications of our observations for the nature and the energy sources of the filaments. Our main conclusions are summarized in Section 5. We assume a distance to M87 of 16.7 Mpc (Blakeslee et al. 2009), which implies a linear scale of 81 pc arcsec^{-1}. The redshift of M87 is $z = 0.004360$.

2. OBSERVATIONS AND DATA ANALYSIS

2.1. Far-infrared Spectroscopy with Herschel PACS

We observed the FIR cooling lines of [C II]λ157 μm, [O I]λ63 μm, and [O IB]λ145 μm with the PACS integral-field spectrometer (Poglitsch et al. 2010) on the *Herschel Space Observatory* (Pilbratt et al. 2010). The observations, with a duration of 10,880 s, were performed on 2012 January 4 (ObsID 1342236278). Table 1 gives a summary of the observations. Columns list the observed lines, their rest frame wavelengths, observation durations, the observed line fluxes and the 2σ upper limits, the spectral resolution full width at half-maximum (FWHM) of the instrument at the given wavelength, the observed FWHM, and the observed line shift with respect to the systemic velocity of M87 ($v = 1307$ km s^{-1}).

The observations were taken in line spectroscopy mode with chopping-nodding to remove the telescope background, sky background, and dark current. A chopper throw of 6′ was used. All three line observations were taken in pointed mode centered on (α, δ) = (12:30:51.5, +12:23:07) (J2000).

The observations were reduced using the `HIPE` software version 8.2.0, using the PACS `ChopNodLineScan` pipeline script for pointed observations. This script processes the data from level 0 (raw channel data) to level 2 (flux calibrated spectral cubes).

During the final stage of reduction the data were spectrally and spatially rebinned into a 5 × 5 × λ cube. In the following we will refer to this cube as the rebinned cube. Each spatial pixel, termed *spaxel*, in this cube has a size of 9.″4 × 9.″4. The cube thus provides us with a field of view (FoV) of 47″ × 47″.

For the wavelength re-gridding we set the parameters *oversample* and *upsample* equal to 2 and 1, respectively. This means that one spectral bin corresponds to the native resolution of the PACS instrument (see the PACS Data Reduction Guide[11] for further information). Larger values for both these two parameters were investigated and did not change the results.

For the [C II] line we projected the rebinned cube onto the sky using the `specProject` task in HIPE and the `hrebin` task in `IDL`. In the following we will refer to this cube as the projected cube. Upon projecting the observed [C II] data from the telescope frame to the sky we have chosen a resolution of 6″ in order to Nyquist sample the beam, the FWHM of which is 12″ at the observed wavelength of the line. We only consider spatial bins where the signal-to-noise ratio of the integrated [C II] flux is greater than 2.

2.2. HST Hα+[N II] and FUV Data

To study the detailed morphology of the filamentary emission-line nebulae, we have also analyzed Hα+[N II] images taken

[11] http://herschel.esac.esa.int/twiki/pub/Public/PacsCalibrationWeb/PDRG_Spec_May12.pdf

with the Wide Field Planetary Camera 2 (WFPC2) through the F658N filter for 2700 s (proposal ID: 5122). The central wavelength of the filter is at 6591 Å and its bandwidth is 29 Å. It transmits the Hα line at $\lambda = 6563$ Å, with transmission $T = 0.80$, and two [N II] lines at $\lambda = 6584$ Å, with $T = 0.20$ and at $\lambda = 6548$ Å, with $T = 0.76$, at the systemic velocity of M87 ($v = 1307$ km s^{-1}). We subtracted the emission of the underlying stellar population of the galaxy using a red continuum image taken with WFPC2 through the filter F814W (proposal ID: 5941).

A FUV image was obtained using the Advanced Camera for Surveys Solar Blind Channel (ACS/SBC; proposal ID: 11861) through the filter F150LP (1630 s), which covers the C IV line at $\lambda = 1549$ Å (see Sparks et al. 2009).

2.3. Chandra X-Ray Data

Extensive *Chandra* X-ray observations of M87 were made between 2002 July and 2005 November using the Advanced CCD Imaging Spectrometer (ACIS). The total net exposure time after cleaning is 574 ks. The data reduction is described in Million et al. (2010). We extracted six background subtracted, flat-fielded, narrow band images between 0.3 keV and 2.0 keV with a 0.492×0.492 arcsec^2 pixel scale (raw detector pixels). To measure the detailed properties of the soft X-ray emission, we also extracted spectra from regions determined using the Contour Binning algorithm (Sanders 2006), as described in Werner et al. (2010). Spectral modeling has been performed with the SPEX package (Kaastra et al. 1996) in the 0.5–7.0 keV band.

2.4. Long Slit Optical Spectra

Long slit spectroscopy was performed using the Intermediate dispersion Spectrograph and Imaging System (ISIS) at the 4.2 m WHT on the island of La Palma on 2011 February 10. The total on-source integration time was 3500 s, split into seven exposures, for the blue and red arm simultaneously. The data were reduced using standard IRAF (Image Reduction and Analysis Facility) procedures. The CCD images were bias subtracted, flat fielded, wavelength calibrated, flux calibrated, and merged. Spectra were shifted into the heliocentric velocity frame. Cosmic rays were removed with the CRNEBULA subroutine, designed for diffuse objects. Blue and red arm images were treated separately during the whole analysis.

3. RESULTS

3.1. Cold and Warm Gas Phases

We detect the filamentary emission-line nebulae across all wavebands studied, from the FIR to the soft X-rays. Using *Herschel* PACS, we detect [C II]λ157 μm line emission (see Figure 1) and determine 2σ upper limits for the [O I]λ63 μm and [O IB]λ145 μm cooling lines. The properties of the FIR lines, spatially integrated over the 5×5 spaxel ($47'' \times 47''$) *Herschel* PACS FoV, are summarized in Table 1. The 2σ upper limits on the fluxes of the [O I]λ63 μm and [O IB]λ145 μm lines given in Table 1 were determined assuming that their velocity widths are equal to the FWHM of the [C II] line.

The [C II]λ157 μm line emission is extended and spatially coincident with the Hα+[N II] filaments (see the top left panel of Figure 2). We see two prominent filamentary structures, which we will call the "southern filament" and the "northern filament." The brightest southern filamentary structure falls

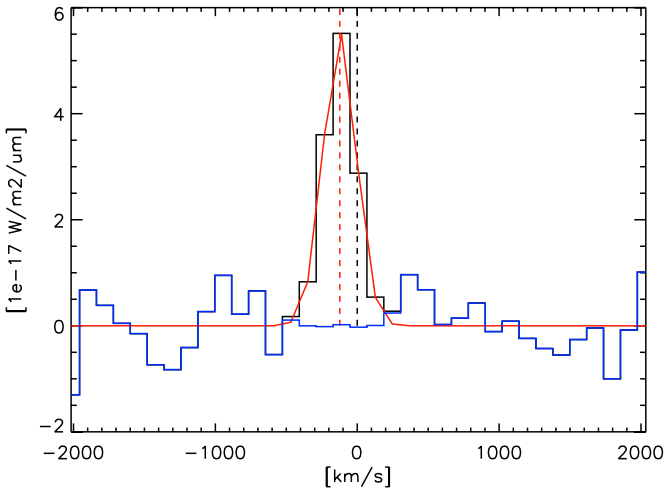

Figure 1. The FIR [C II]λ157 μm line obtained from the central spaxel (9.4×9.4 arcsec^2) of the *Herschel* PACS rebinned data cube. The mean line centroid is blueshifted with respect to M87 (at $z = 0.004360$) by $v = -123 \pm 5$ km s^{-1}. The blue line indicates the detector noise.

(A color version of this figure is available in the online journal.)

on the central spaxel of the PACS spectrometer. The [C II] flux detected from the central spaxel (9.4×9.4 arcsec^2) in the rebinned cube is $(8.5 \pm 0.7) \times 10^{-15}$ erg s^{-1} cm^{-2}. The top central panel of Figure 2 shows a map of the velocity distribution of the [C II] line emitting gas with respect to the velocity of M87. This image shows an interesting dichotomy, with the northern filaments receding at about +140 km s^{-1} and the bright southern filament (most of the emission of which falls on the central 9.4×9.4 arcsec^2 spaxel of the detector) moving in the opposite direction along our line of sight at -123 ± 5 km s^{-1}, with respect to M87. These velocities show good agreement with the radial velocities of the corresponding optical filaments measured using long-slit spectroscopy (Sparks et al. 1993). The top right panel of Figure 2 shows a map of the velocity dispersion of the [C II] line emitting material. While the northern, receding filaments show a significant velocity dispersion of $\sigma = \mathrm{FWHM}/2.355 \sim 124$ km s^{-1} (FWHM $= \sqrt{377^2 - 240^2} = 291$ km s^{-1}, corrected for the instrumental resolution FWHM of 240 km s^{-1}), the velocity dispersion measured in the southern filaments, $\sigma \sim 55$ km s^{-1} (FWHM $= \sqrt{273^2 - 240^2} = 130$ km s^{-1}), is just marginally above the instrumental resolution.

The middle row left panel of Figure 2 shows the Hα+[N II] image obtained with *HST* WFPC2. Contours of 6 cm radio emission from Hines et al. (1989) are over-plotted, showing that in projection the side of the southern filament closest to the nucleus overlaps with the radio lobes. The narrowest resolved filaments of Hα+[N II] emission have a diameter of only $0\farcs4$, which corresponds to 32 pc. The total count rate measured in our narrow band image from the bright southern filamentary structure within a $15\farcs7 \times 5\farcs7$ box-like region centered at $(\alpha, \delta) =$ (12:30:51.48,+12:23:07.33) is 6.94 counts s^{-1}. Assuming an [N II]λ6548/Hα flux ratio of 0.81 and [N II]λ6584/Hα = 2.45 (Ford & Butcher 1979) and taking into account the filter throughput at the wavelengths of the lines (see Section 2.2), the Hα flux of the southern filament is $f_{\mathrm{H}\alpha} = 9.0 \times 10^{-15}$ erg s^{-1} cm^{-2}.

Sparks et al. (2009) reported that the Hα+[N II] emission-line nebulae are co-spatial with FUV emission (see the middle row central panel of Figure 2). Using subsequent spectroscopic measurements with the *HST* Cosmic Origin Spectrograph, Sparks et al. (2012) showed that the FUV emission in the

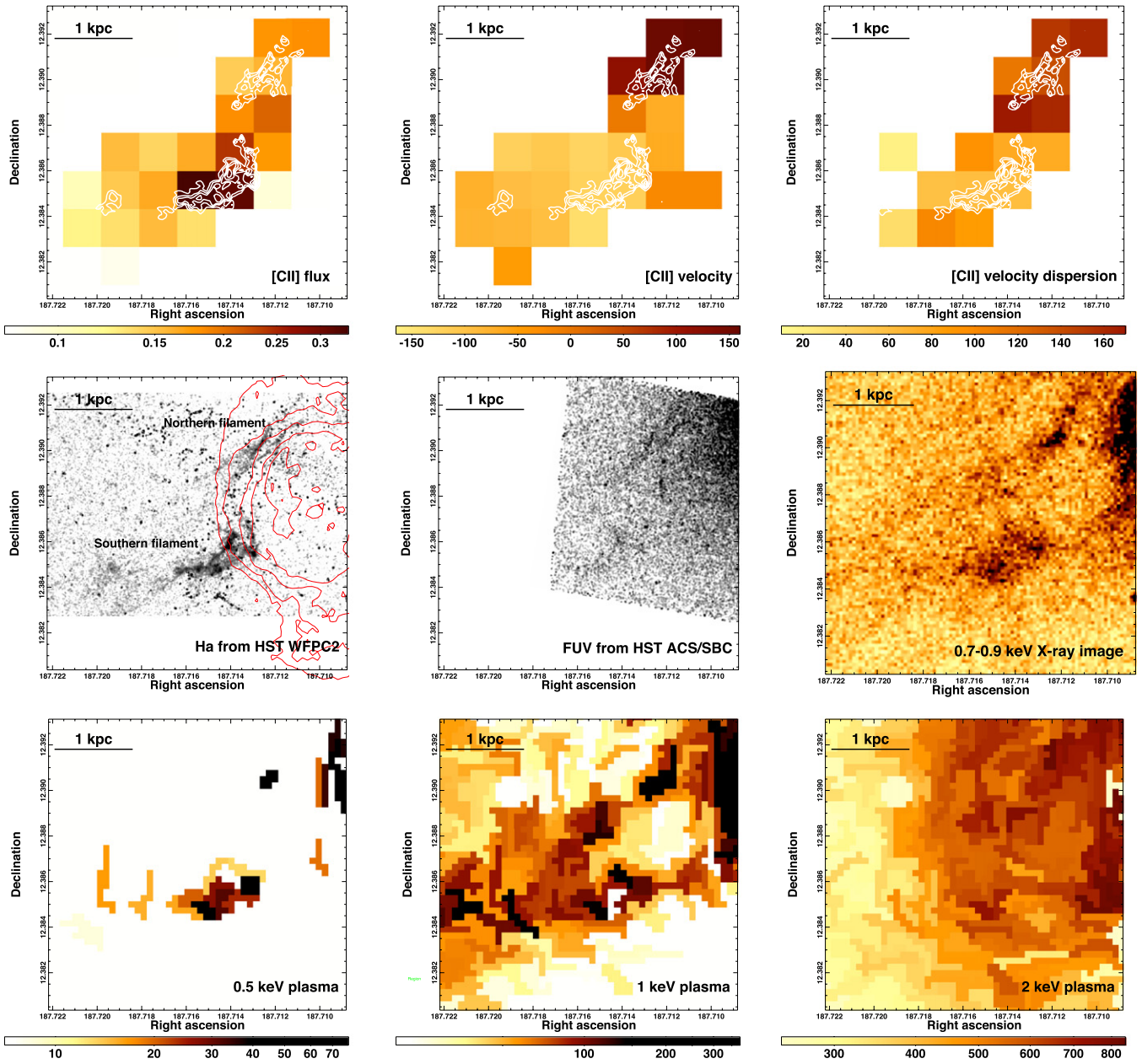

Figure 2. FIR [C II] maps (top panels; we only show spatial bins where the signal-to-noise ratio of the integrated [C II] flux is greater than 2) and Hα+[N II], FUV, and X-ray images of the filamentary multi-phase gas southeast of the nucleus of M87. All images show the same 47 × 47 arcsec region of the sky. The projected distance of the bright filaments from the nucleus is 38″ (3 kpc). Top left panel: map of the integrated [C II] line flux in units of 10^{-14} erg s^{-1} cm^{-2} per 6″ × 6″ spaxel obtained with *Herschel* PACS. Top central panel: the velocity distribution of the [C II] emitting gas, in units of km s^{-1}, relative to the systemic velocity of M87, $v = 1307$ km s^{-1}. Top right panel: map of the velocity dispersion, σ, of the [C II] emitting gas. Middle row left panel: Hα+[N II] image obtained with *HST* WFPC2. The contours of these filaments are over-plotted on the *Herschel* PACS maps in the top row. On this *HST* WFPC2 image, contours of 6 cm radio emission from Hines et al. (1989) are over-plotted in red. Middle row central panel: FUV image showing C IV line emission obtained with *HST* ACS/SBC. Middle row right panel: *Chandra* soft X-ray image, extracted in the 0.7–0.9 keV band. Bottom panels: spatial distribution of the emission measure, $Y = \int n_{\rm H} n_{\rm e} dV$ (in 10^{58} cm^{-3} arcsec^{-2}), of the 0.5 keV (bottom left), 1.0 keV (bottom central), and 2.0 keV (bottom right) plasma detected at 99.7% confidence.

(A color version of this figure is available in the online journal.)

northern filaments is due to C IV line emission. We find that the C IV flux, measured within the same aperture as the Hα+[N II] flux above, is $f_{\rm C\,IV} = 1.2 \times 10^{-14}$ erg s^{-1} cm^{-2}.

The optical spectral properties of the southern filament show an intriguing rapid decrease in the [O III]/Hβ ratio with increasing distance from the nucleus, dropping monotonically from ∼2.5 at a projected distance of 28″ to ∼0.7 at 43″ (see Figure 3). The diagram in the left panel of Figure 3, showing the [O III]/Hβ over the [N II]/Hα ratios (a BPT diagram; Baldwin et al. 1981), indicates that the side of the filament closest to the nucleus, which also overlaps with the radio lobes (see middle row left panel of Figure 2), has spectra similar to Seyfert-like active galactic nuclei (AGNs). The [O III]/Hβ line ratios in this part of the filament are larger than in the nucleus of M87, where we measure a ratio of ∼1.75. At larger radii, the gas has a LINER[12]-like emission spectrum, which is more similar to the emission line spectra typically seen in extended filaments around brightest cluster galaxies in cluster cores.

[12] Low-ionization nuclear emission-line region (Heckman 1980).

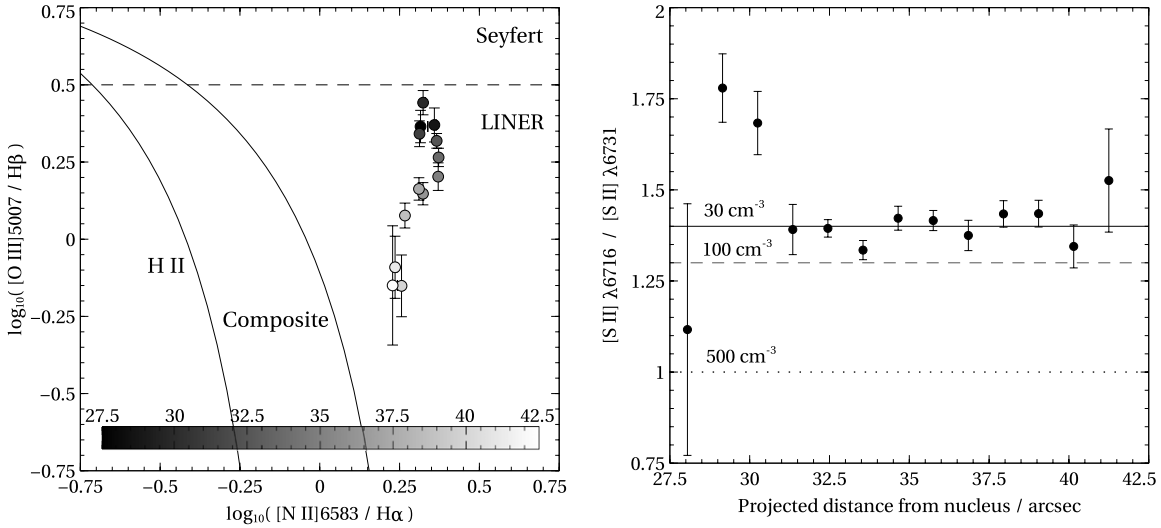

Figure 3. Left panel: optical diagnostic diagram (a BPT diagram; Baldwin et al. 1981) showing the [O III]/Hβ against the [N II]/Hα flux observed in the southern filament at different radii from the nucleus. The brightening shades of gray indicate increasing projected distance from the nucleus in arcsec. While the side of the filament closest to the nucleus has spectra similar to Seyfert-like AGN, at larger radii the gas has a LINER-like emission spectrum. The solid and dashed lines are from Kewley et al. (2006) and Osterbrock & Ferland (2006), respectively. Right panel: the measured [S II]λ6716/[S II]λ6731 line ratios, a good probe of gas density, as a function of radius. The full, dashed, and dotted lines indicate ratios corresponding to electron densities of $n_e = 30$ cm^{-3}, $n_e = 100$ cm^{-3}, and $n_e = 500$ cm^{-3}, respectively (Osterbrock & Ferland 2006).

The right-hand panel of Figure 3 shows the measured [S II]λ6716/[S II]λ6731 line ratio, a good probe of gas density, as a function of radius. The full, dashed, and dotted lines indicate ratios corresponding to electron densities of $n_e = 30$ cm^{-3}, $n_e = 100$ cm^{-3}, and $n_e = 500$ cm^{-3}, respectively (Osterbrock & Ferland 2006). The value $n_e = 30$ cm^{-3} is very close to the low density limit, below which the [S II] line ratios do not provide useful constraints on gas density. Along most of the filament, the line ratios are close to this limit, indicating that the electron density of the 10^4 K phase is $n_e \lesssim 30$ cm^{-3}. At radii between 29″ and 30.″5, the measured line ratios are outside of the low density limit. The data point closest to the nucleus, at 28″, indicates a possible increase in density, but with large error bars.

3.2. The Soft X-Ray Emission

Young et al. (2002) and Sparks et al. (2004) found good spatial correlation between Hα+[N II] line emission and soft X-ray emission. Here, we have analyzed almost four times as much *Chandra* data, which provides excellent photon statistics in the regions of interest. We extracted six narrow band images between 0.3 keV and 2.0 keV and found that the filaments stand out clearly in the 0.7–0.9 keV band (see the middle row right panel of Figure 2). The spatial correlation between the 0.7–0.9 keV X-rays and the Hα+[N II] line emission is remarkable: everywhere we see Hα+[N II] emitting gas, we also see an excess of soft X-rays. On the other hand, in the 0.5–0.7 keV and 0.9–1.2 keV bands the filaments do not stand out clearly against the surrounding emission, indicating that most of their X-ray emission comes from the Fe XVII and Fe XVIII lines in the 0.7–0.9 keV band. The excess X-ray flux of the filaments in this band is 1.1×10^{-14} erg s^{-1} cm^{-2} and their average X-ray surface brightness is 1.2×10^{-16} erg s^{-1} cm^{-2} arcsec^{-2}.

Assuming that the soft X-ray emission is of a thermal origin, we follow the analysis of Werner et al. (2010) and fit to each spatial bin a model consisting of collisionally ionized equilibrium plasmas at three fixed temperatures (0.5 keV, 1.0 keV, and 2.0 keV), with variable normalizations and common metallicity. The bottom panels of Figure 2 show the spatial distributions of the emission measures of the individual temperature components. The 0.5 keV component closely follows the distribution of the cold gas phases. This component is required to fit the Fe XVII and Fe XVIII lines in the 0.7–0.9 keV band, which are only present in regions where Hα+[N II] emission has also been detected. The spatial correlation between Hα+[N II] and the softest X-ray emitting component is, however, not perfect: the ratio of Hα+[N II] flux to the ~0.5 keV emission component is ~5 times larger in the southern than in the northern filament. The 1 keV component is enhanced as well in the regions where cold gas is present, but it is spatially more extended and is also seen in many regions where cold gas is not detected (see Werner et al. 2010). The spatial distribution of the 2 keV plasma does not correlate with the Hα+[N II] emission.

Because the soft X-ray line emission observed in the filaments may be due to cooling gas, we fitted the spectra with a model consisting of a single-temperature plasma in collisional ionization equilibrium plus an isobaric cooling flow, which models cooling between two temperatures at a certain metallicity and mass deposition rate. The upper temperature and the metallicity of the cooling flow component were tied to the temperature and metal abundance of the single-temperature plasma. Both components were absorbed by a Galactic absorption column density $N_H = 1.9 \times 10^{20}$ cm^{-2} (Kalberla et al. 2005). Fixing the lower temperature cutoff of the cooling flow model to $kT_{low} = 0.5$ keV, we obtained a best-fit upper temperature of $kT_{up} = 1.90 \pm 0.04$ keV, a mass deposition rate of $\dot{M} = (2.46 \pm 0.13) \times 10^{-2}\, M_\odot$ yr^{-1}, and a metallicity of $Z = 1.46 \pm 0.09$ solar (relative to the solar values by Grevesse & Sauval 1998). Even though the spectra indicate that above $kT \sim 0.5$ keV the gas may be cooling, the spectral signatures of gas cooling below 0.5 keV—soft X-ray emission, including the O VII line—are missing (see also the high resolution spectra in Werner et al. 2006, 2010).

In order to test whether the missing soft X-ray flux might have been absorbed by the cold gas in the filaments, we fixed the mass deposition rate in the model to the best fit value obtained with

a lower temperature cutoff set to 0.5 keV and extended this cutoff down to a 1000 times lower temperature of 0.5 eV (the lowest value allowed by the model). Furthermore, we assumed that the cooling X-ray plasma is intermixed with the cold gas and the cooling happens in 13 different regions along our line-of-sight separated from each other by intrinsic cold absorbers (the emission from the first cooling region is affected by one absorber, from the second by two absorbers, from the third by three, etc.). The different cooling regions are assumed to have the same cooling rate and the different absorbers are assumed to have the same hydrogen column density. Fitting this model to the data, we find an integrated intrinsic hydrogen column density of $N_{\rm H} = (1.58 \pm 0.21) \times 10^{21}$ cm^{-2} and an absorbed bolometric flux of 3.9×10^{-14} erg s^{-1} cm^{-2}.

4. DISCUSSION

4.1. Magnetized Filaments of Multi-phase Material

In the filamentary emission-line nebulae to the southeast of the nucleus of M87, we detect gas spanning a temperature range of at least five orders of magnitude, from ∼100 K to ∼10^7 K. The [C II], Hα+[N II], and C IV emitting gas phases are consistent with being co-spatial, forming a multi-phase medium. Soft X-ray emission in the 0.7–0.9 keV band is also always present in regions where Hα+[N II] emission is seen. Its spectral shape is consistent with line emission of ∼0.5 keV thermal plasma, previously detected in the *XMM-Newton* high-resolution reflection grating spectra integrated over the central region of M87 (Werner et al. 2006, 2010). We see no evidence of X-ray emitting gas with temperature $kT < 0.5$ keV.

The [C II] 158 μm line is about 1500 times stronger than the CO (1→0) rotational line in normal galaxies and Galactic molecular clouds, and 6300 times more intense in starburst galaxies and Galactic star-forming regions (Crawford et al. 1985; Stacey et al. 1991). Given a [C II] flux of 8.5×10^{-15} erg s^{-1} cm^{-2} observed from the brightest region of the southern filament, the expected CO (1→0) flux is 1.3–5.3 $\times 10^{-18}$ erg s^{-1} cm^{-2}, consistent with the upper limit of 2×10^{-17} erg s^{-1} cm^{-2} for CO (1→0) at 2.6 mm observed in the same region (Salomé & Combes 2008). Using the standard CO luminosity to H_2 conversion factors the inferred range of CO luminosities corresponds to an H_2 mass of 0.4–2 $\times 10^6$ $M_\odot$. However, because the [C II]/CO line ratios in these filaments may be different from those in star-forming galaxies and their heating mechanism may be different from that in more normal molecular clouds, their true molecular mass may be outside of this range.

Assuming that all the observed gas phases are in thermal pressure equilibrium with the ambient ICM (assuming p = 0.11–0.22 keV cm^{-3}, for a distance range of r = 3–6 kpc from the nucleus depending on the position of the filament along our line of sight; Churazov et al. 2008), the ∼100 K [C II] emitting gas forms a network of narrow filaments with densities of the order of (1.3–2.6) $\times 10^4$ cm^{-3} (higher than the critical density of 3×10^3 cm^{-3} above which the gas is in local thermal equilibrium with the level populations determined by collisions) with volume filling fraction of $f_{\rm V} \sim$ (1–2) $\times 10^{-4}$ in the bright southern filament. Although the presence of O I 6300 Å lines in the optical spectra (see also Ford & Butcher 1979) indicates the existence of large partially ionized regions in the filaments, the presence of [S II] lines most probably indicates a fully ionized ∼10^4 K phase surrounding the colder gas. The density of this Hα+[N II] emitting gas, assuming thermal pressure equilibrium with the ambient ICM, should be ∼(1.3–2.6) $\times 10^2$ cm^{-3}.

The [S II]λ6716/[S II]λ6731 line ratios, however, indicate much lower particle densities in the 10^4 K phase ($n \sim 2n_{\rm e} \lesssim 60$ cm^{-3}) implying the presence of additional significant non-thermal pressure components in the filaments, such as turbulence and magnetic fields. Assuming isotropic microturbulence with a characteristic velocity $v_{\rm turb}$ in a medium with a sound speed $c_{\rm s}$, the turbulent pressure support will be $p_{\rm turb} = 1/2\,\gamma\ p_{\rm therm}\ M^2$, where γ is the adiabatic index assumed to be 5/3 and $M = v_{\rm turb}/c_{\rm s}$ is the Mach number. However, assuming characteristic turbulent velocities of the order of the sound speed in the 10^4 K phase ($c_{\rm s}$ = 15 km s^{-1}), the sum of thermal and turbulent pressure, $p_{\rm turb} + p_{\rm therm}$ = 0.09 keV cm^{-3} (1.4×10^{-10} dyne cm^{-2}), is still smaller than the surrounding ICM pressure. If the turbulence in the Hα emitting phase is subsonic, then the additional pressure will be provided by magnetic fields. A magnetic pressure of $p_{\rm mag} = B^2/8\pi \sim$ (0.3–2.1) $\times 10^{-10}$ dyne cm^{-2}, needed to keep the filaments in pressure equilibrium with the surrounding ICM, requires magnetic fields of B = 28–73 μG. This is similar to the values inferred using arguments based on the integrity of Hα+[N II] filaments in the Perseus Cluster (Fabian et al. 2008). Radio observations of the Faraday rotation measure in a number of cooling cores revealed magnetic field strengths of 10–25 μG (Taylor et al. 2001, 2007; Allen et al. 2001; Feretti et al. 1999). Significant imbalance in thermal pressure of the gaseous filaments in cool-core clusters has previously also been inferred between the warm molecular hydrogen gas seen in NIR ($nT \sim 10^8$–10^9 cm^{-3} K) and the ionized gas phases seen in the optical ($nT \sim 10^5$ cm^{-3} K), emphasizing the need for dynamic models for the filaments (Jaffe et al. 2001; Oonk et al. 2010).

The smallest resolved diameter of the Hα+[N II] filaments is 32 pc, about half of the 70 pc diameter observed in the more distant Perseus Cluster (Fabian et al. 2008). However, even the narrowest resolved filaments are likely to consist of many smaller strands. They are surrounded by hotter 10^5 K C IV emitting gas. The space between these filaments is filled by X-ray emitting gas. If the soft X-ray line emission is due to ∼0.5 keV gas, then based on our three-temperature fits (see Section 3) and assuming thermal pressure equilibrium with the ambient ICM, its mass in the southern filament is ∼10^5 $M_\odot$ and its emitting volume is ∼0.016 kpc^3.

4.2. The Energy Source of the Filaments

Sparks et al. (2009) show that no main-sequence stars of early spectral type are present in the filaments and therefore neither the FUV nor the Hα+[N II] emission can be due to photoionization by hot UV emitting stars. The [O III]/Hβ emission line ratios are high on the side of the southern filament closest to the nucleus, which also overlaps with the radio lobes (see middle row left panel of Figure 2), and then decrease rapidly with increasing distance from the nucleus. The fact that the line ratios in the filament reach values that are higher than those measured in the nucleus argues against photoionization by the AGN. It seems more likely that the increased [O III]/Hβ ratios are due to internal shocks produced as the radio lobes push against the cold gas. These shocks seem to affect only a part of the filament and the emitted Hα flux does not decrease with the decreasing [O III]/Hβ emission line ratios. Therefore, they can be ruled out as energy source powering the emission of these nebulae.

Ferland et al. (2009) showed that the broad band (optical to mm) emission-line spectra of nebulae around central galaxies

of cooling core clusters most likely originate in gas exposed to ionizing particles. Such ionizing particles can be either relativistic cosmic rays or hot particles penetrating into the cold gas from the surrounding ICM. Saturated conduction from the hot into the cold phase of the southern filament would produce a heat flux of $5\phi p c_s \sim 0.1$ erg s^{-1} cm^{-2}, where $\phi \sim 1$ accounts for the uncertain physics, $p = 0.22$ keV cm^{-3} is the gas pressure and $c_s = 510$ km s^{-1} is the sound speed in the hot 1 keV phase (Cowie & McKee 1977; Fabian et al. 2011). Following the argument of Fabian et al. (2011), given a typical Hα surface brightness of $\sim 2 \times 10^{-16}$ erg s^{-1} cm^{-2} arcsec^{-2}, corresponding to an emitted flux of 1.1×10^{-4} erg s^{-1} cm^{-2} and assuming that the total broad band emitted flux is 20 times larger 2.2×10^{-3} erg s^{-1} cm^{-2}, the required efficiency with which impinging thermal particles penetrate and excite the cold gas is of the order of $f = 0.022$ ($f = 0.044$ for a filament at $r = 6$ kpc from the nucleus), which is reasonable. However, these particles must somehow overcome the obstacle presented by the magnetic fields believed to be at the interface of the cold and hot gas phases.

Werner et al. (2010) show that all of the bright Hα+[N II] and UV filaments are seen in the downstream region of a <3 Myr old AGN induced $M \gtrsim 1.2$ shock front (Million et al. 2010) that seems to have just passed the filaments. Based on these observations they propose that shocks induce shearing around the cold, filamentary, dense gas, thereby promoting mixing of the cold gas with the ambient hot ICM via instabilities (e.g., Friedman et al. 2012). Instabilities and turbulence may also be driven by shearing motions between the hotter X-ray gas and the filaments, as they move through the ambient ICM, both as they are being uplifted and as they fall back. This type of more continuous shear induced mixing could perhaps be in the long term more important for energizing the filaments than shocks. Fabian et al. (2011) propose that the submillimeter through UV emission seen in NGC 1275 in the core of the Perseus Cluster is due to the hot ICM efficiently penetrating the cold gas through reconnection diffusion (Lazarian et al. 2010, 2011). The same process may also be operating in the filaments of M87 with the fast reconnection induced by shearing instabilities and turbulence. Shearing and magnetic reconnection are, however, not essential to bring the cold gas into contact with the hot ICM. The support from magnetic fields tied to the surrounding ionized phase may become unstable if the layer of dense cold neutral gas is deep enough, and therefore it may fall through into direct contact with the hot gas. The hot ICM particles penetrating the cold gas then produce secondary electrons that excite the observed FIR through UV emission as shown by Ferland et al. (2009). Mixing of the cold and hot gas also naturally account for the presence of the $\sim 10^5$ K intermediate-temperature gas phase (geometric mean of the hot and cold gas temperatures) predicted by the mixing layers calculated by Begelman & Fabian (1990), although mixing layers have most probably a more complicated temperature structure (Esquivel et al. 2006). As the X-ray emitting gas cools through mixing, the mass of the southern filament may grow by as much as $4 \times 10^{-2}\ M_\odot$ yr^{-1}.

The particle heating model of Ferland et al. (2009), calculated considering optically thin emission from a cell of gas, predicts [O I]/[C II] $\sim$ 21 and is inconsistent with the 2σ upper limit of 7.2 observed in M87. The ratios observed in the Perseus and Centaurus clusters, and in A1068 and A2597 are even lower. This discrepancy has been discussed in a recent study of NGC 1275 by Mittal et al. (2012), who conclude that the line ratio suggests that the lines are optically thick, implying a large reservoir of cold atomic gas, which was not accounted for in previous inventories of the filament mass. The same can be concluded for M87, where the large optical depth of the FIR lines (R. E. A. Canning et al. 2013, in preparation) and the intrinsic absorption inferred from the X-ray data (see below) imply significant reservoirs of cold atomic and molecular gas.

4.3. X-Ray Line Emission from Cold Gas Due to Charge Exchange and Inner Shell Ionization?

As ions from the hot ICM penetrate into the filaments, they pick up one or more electrons from the cold gas. The impinging ions thus get into excited states and their deexcitation may produce X-ray radiation. Astrophysical X-ray emission due to this "charge exchange" process was first discovered in the comet Hyakutake (Lisse et al. 1996; Cravens 1997) and since then it has been identified as the mechanism responsible for X-rays from planets (e.g., Gladstone et al. 2002; Dennerl 2002), the geocorona (Wargelin et al. 2004; Fujimoto et al. 2007), the heliosphere (Robertson et al. 2001), and interstellar medium in particular at interfaces between hot gas and cool clouds (see the review by Dennerl 2010, and references therein). Recently, charge exchange has also been found to possibly contribute significantly to the soft X-ray line emission from star-forming galaxies (Liu et al. 2011, 2012). Fabian et al. (2011) conclude that in the Perseus Cluster charge exchange may account for a few per cent of the soft X-ray emission from the filaments. They also speculate that if the filaments are composed of many small strands, the same ion might pass from the hot into the cold and back to the hot phase repeatedly, getting collisionally ionized while passing through the hot ICM, thus enhancing the charge exchange emission to the observed level.

After hydrogen and helium, the most abundant ions penetrating the cold gas are O^{8+}, C^{6+}, N^{7+}, Ne^{10+}, Mg^{12+}, Mg^{11+} (with concentrations 8.4×10^{-4}, 3.6×10^{-4}, 1.1×10^{-4}, 1.1×10^{-4}, 2.5×10^{-5}, 1.07×10^{-5} relative to hydrogen by number). Charge transfer onto these ions is expected to produce mainly hydrogen and helium like line emission in the X-ray band. In the 1 keV plasma surrounding the filaments, 23% of Fe is in the form of Fe^{20+}, another 23% in Fe^{21+}, 18% in Fe^{19+}, and 17% in Fe^{22+}, with relative concentrations smaller than 1.1×10^{-5}. The charge exchange line fluxes produced by Fe will therefore be significantly lower, with most of the line flux in Fe XIX to Fe XXII lines, in the spectral band above 0.9 keV. Moreover, laboratory measurements of X-ray spectral signatures of charge exchange in L-shell Fe ions by Beiersdorfer et al. (2008) found that the $n \geqslant 4 \rightarrow n = 2$ transitions are strongly enhanced relative to $n = 3 \rightarrow n = 2$, shifting the line emission to higher energies. Because charge transfer processes and the corresponding X-ray emission are expected to occur inside of the dense cold clouds, absorption may significantly decrease the observed fluxes of the lowest energy X-ray lines such as C VI, N VII, O VII, and O VIII. The Ne IX, Ne X, Mg XI, and Mg XII lines in the 0.9–1.9 keV band are, however, not expected to be affected by absorption strongly and their enhancement might indicate charge exchange. Given that none of these lines are enhanced in the filaments, and no strong charge exchange emission is expected in the 0.7–0.9 keV band, we conclude that the observed soft X-ray emission is not due to charge transfer onto the impinging ions.

The ions and electrons penetrating from the surrounding hot ICM into the cold filaments will also ionize the inner electron shells of the atoms and molecules in the cold clouds. This inner shell ionization may in principle also contribute to the X-ray

emission of the filaments, but given the energetics, it is not expected to be significantly stronger than the X-ray emission due to charge exchange. We would primarily expect to see X-ray lines from few times ionized C, N, O, Ne, and Mg, with the Ne and Mg lines in the band above 0.6 keV. Detailed predictions of this process are beyond the scope of this paper.

Given that the spectral shape of the filaments is consistent with line emission of ∼0.5 keV thermal plasma previously resolved within the central region of M87 with *XMM-Newton* reflection grating spectrometers (Werner et al. 2006, 2010) and that charge exchange as a significant source of X-ray emission from the filaments can be ruled out, we conclude that the observed soft X-ray emission is most likely due to thermal plasma. We note, however, that although charge exchange is not responsible for the observed excess X-ray emission in the 0.7–0.9 keV band, the level that is required from the particle heating model is observationally acceptable.

4.4. AGN Uplift Induced Cooling Instabilities or Mixing?

The observed velocity distribution of the [C II] (see top central panel of Figure 2) and optical emission lines (Sparks et al. 1993) indicates that the northern filaments are currently being uplifted by the counter-jet (which is oriented at $<19^{\circ}$ from our line-of-sight; Biretta et al. 1999) moving away from M87 with a line-of-sight velocity of $v_{\rm LOS} = +140$ km s^{-1}. The southern filaments, in contrast, are falling back toward M87 with $v_{\rm LOS} = -123$ km s^{-1}. Assuming uplift at the Keplerian velocity of ∼400 km s^{-1}, the southern filament would take 8×10^6 yr to get to its current position. Given that this filament is most likely already falling back, its age is $\gtrsim 10^7$ yr. Uplift of low entropy, metal enriched X-ray emitting gas by buoyantly rising relativistic plasma from the AGN jets of M87 has been previously inferred based on radio and X-ray data (Churazov et al. 2001; Forman et al. 2005; Simionescu et al. 2008; Werner et al. 2010). Optical emission line nebulae also appear to have been drawn out by rising radio bubbles in other nearby systems (e.g., the Perseus and Centaurus clusters; Hatch et al. 2006; Canning et al. 2011).

The initially uplifted material might have already been a multi-phase mixture of low entropy X-ray emitting plasma and dusty cold gas, as is observed in the core of M87 (Sparks et al. 1993). As the relatively dense, low entropy X-ray emitting plasma was removed from the direct vicinity of the AGN jets it might have cooled radiatively, further contributing to the cold gas mass of the uplifted material (see Revaz et al. 2008). The multi-phase X-ray emitting gas, with the 0.5 keV phase co-spatial with the Hα+[N II] filaments and surrounded by a spatially more extended 1 keV plasma, indicates that such cooling may be taking place. Cooling instabilities are predicted to take place in cooling core clusters within radii where the ratio of the cooling time to free fall time is $t_{\rm cool}/t_{\rm ff} \lesssim 10$ (Sharma et al. 2012; McCourt et al. 2012; Gaspari et al. 2012, this condition is fulfilled at the radii where the M87 filaments are seen). AGN induced uplift of multi-phase gas may facilitate the onset of such local cooling instabilities. Some Hα+[N II] and soft X-ray filaments lie at the edges of cavities filled by radio emitting plasma, indicating that they might be sheets of gas seen in projection that have been swept up and compressed by the expanding and rising cavities. Even though such compression would first heat the gas, eventually it will accelerate its cooling. This picture of radiatively cooling X-ray gas is, however, complicated by the observed temperature floor at 0.5 keV. Several explanations were proposed to address the missing soft X-ray emission, including mixing (Fabian et al. 2002), anomalous O/Fe abundance ratios, and absorption (Sanders & Fabian 2011).

The mass deposition rate, inferred from the temperature distribution of the X-ray gas in the southern filament above $kT = 0.5$ keV, assuming an isobaric cooling flow model, is $\dot{M} = (2.46 \pm 0.13) \times 10^{-2}\, M_{\odot}$ yr^{-1}. This cooling rate could only be reconciled with the apparent lack of $kT < 0.5$ keV plasma if the cold gas in the filaments absorbs the soft X-rays, modifying the observed spectral shape in a way that results in an apparent temperature cutoff. The X-ray spectral lines providing the most diagnostic power at these temperatures are the Fe XVII and the O VII lines. The ionic fraction of Fe XVII is above 0.3 across a relatively large temperature range of 0.2–0.6 keV, but the O VII line becomes observable only at $kT < 0.4$ keV. Absorption is expected to strongly suppress the O VII line emitted by the coldest gas phases. The Fe XVII lines will be affected by absorption to a much lesser extent. Therefore when modeling a spectrum that is affected by intrinsic absorption, we may conclude that the cooling stopped at the temperature where we expect to start to see the O VII line.[13] In Section 3, we show that the required integrated hydrogen column density, distributed in multiple layers (the cooling takes place between the threads) along our line-of-sight is $N_{\rm H} = (1.58 \pm 0.21) \times 10^{21}$ cm^{-2}. If the hot ICM indeed cools radiatively between the cold filaments, then the large area covering fraction of the many small strands may provide a sufficient absorption column to the cooling X-ray emitting plasma to explain the apparent temperature floor at ∼0.5 keV.

Soft X-ray photons from the cooling X-ray plasma absorbed by the cold gas would produce energetic photoelectrons that would contribute to the heating and ionization of the cold gas (in a process similar to the secondary electron production by cosmic rays or impinging hot ICM particles; Ferland et al. 2009). Photoionization of emission line nebulae by X-rays has been considered before (e.g., Heckman et al. 1989; Donahue & Voit 1991; Crawford & Fabian 1992; Jaffe & Bremer 1997) and has been found insufficient to ionize and power the observed line emission. However, when considering photoionization by primarily soft X-rays, from cooling plasma which surrounds the cold filamentary gas with a small volume filling fraction, the efficiency of this process increases significantly (Oonk 2011). According to our spectral modeling, where we assumed that all the soft X-ray emission is due to radiative isobaric cooling, intrinsic absorption reduces the observed flux by $\sim 3.9 \times 10^{-14}$ erg s^{-1} cm^{-2}. If the soft X-ray emitting plasma fills the space between the cold filaments and the cold gas absorbs approximately the same amount of energy in all directions, then the total X-ray energy absorbed by the cold gas is $\sim 1.3 \times 10^{39}$ erg s^{-1}. With a total emitted energy from UV to submillimeter about 20 times larger than the observed Hα luminosity of 3.0×10^{38} erg s^{-1}, X-ray photoionization may, in principle, contribute a significant fraction of the energy needed to power the filaments.

The cooling rates above were deduced under the assumption that all the soft X-ray line emitting gas originates from radiative cooling. The $kT \sim 0.5$ keV gas could, in principle, also be produced by mixing of the hot ICM with the cold filaments. More developed mixing might be responsible for the higher

[13] We note that only a small fraction of the observed X-ray emission originates in the filaments and is affected by intrinsic absorption. The dominant emission component from the ambient ICM remains unaffected by cold gas in the filaments, and therefore fitting the spectra with a Galactic absorption as a free parameter will not result in a significantly higher best fit $N_{\rm H}$.

ratio of 0.5 keV thermal to Hα+[N II] line emission in the southern filament (which is most likely falling back toward M87), with respect to the northern filament (which is likely younger, currently being uplifted). Such mixing is, however, not expected to result in a gas with $kT \sim 0.5$ keV—it would result in a mixing layer with a wide range of temperatures (Esquivel et al. 2006). Therefore, both in the cooling and in the mixing scenario for the origin of the soft X-ray emission from the filaments, the explanation of the 0.5 keV cutoff requires intrinsic absorption by cold gas.

The internal reddening in the optical band calculated from the observed line ratio of Hα/H$\beta = 4$ in the filament (Ford & Butcher 1979) is $E(B-V) = 0.28$. Using the Galactic transformation between reddening and column density of neutral hydrogen, $N_{\rm H}/E(B-V) = 5.8 \times 10^{21}$ cm^{-2} mag^{-1} (Bohlin et al. 1978), we infer an intrinsic neutral hydrogen column density of $N_{\rm H} = 1.6 \times 10^{21}$ cm^{-2}—sufficient to absorb the soft X-ray emission from gas with $kT < 0.5$ keV. We note that substantial reddening has been observed in a number of Hα nebulae in brightest cluster galaxies of cooling core clusters (e.g., Allen et al. 1995; Crawford et al. 1999).

A similar temperature floor at ~0.5 keV is observed in the Perseus Cluster, Centaurus Cluster, 2A 0335+096, A262, A3581, HCG 62, and A2052 (Sanders & Fabian 2007; Sanders et al. 2008, 2009, 2010; de Plaa et al. 2010) and in the cooling uplifted multi-phase gas in the core of the galaxy cluster Sérsic 159-03 (Werner et al. 2011). The coolest ~0.5 keV gas phases are co-spatial with filamentary optical emission-line nebulae in all of these systems. In the Perseus and Centaurus clusters, copious amounts of FIR line emission has also been discovered, indicating the presence of large reservoirs of cold atomic gas (Mittal et al. 2011, 2012). Following the arguments outlined above, the low temperature X-ray cutoffs observed in those systems may therefore also, at least partly, result from intrinsic absorption.

5. CONCLUSIONS

We performed a multi-wavelength study of the emission-line nebulae located southeast of the nucleus of M87. Our main conclusions may be summarized as follows.

1. We detect FIR [C II] line emission at 158 μm with *Herschel* PACS. The line emission is extended and co-spatial with optical Hα+[N II], FUV C IV lines, and soft X-ray emission.
2. The filamentary nebulae contain multi-phase material spanning a temperature range of at least five orders of magnitude, from ~100 K to ~10^7 K. This material has most likely been uplifted by the AGN from the center of M87.
3. The thermal pressure of the 10^4 K phase appears to be significantly lower than that of the surrounding hot ICM indicating the presence of additional turbulent and magnetic pressure in the filaments. If the turbulence in the filaments is subsonic then the magnetic field strength required to balance the pressure of the surrounding ICM is $B \sim 30$–$70\,\mu$G.
4. The spectral properties of the soft X-ray emission from the filaments indicate that it is due to thermal plasma with $kT \sim 0.5$–1 keV, which is cooling by mixing with the cold gas and/or radiatively. Charge exchange can be ruled out as a significant source of soft X-rays.
5. Both cooling and mixing scenarios predict gas with a range of temperatures. This is at first glance inconsistent with the apparent lack of X-ray emitting gas with $kT < 0.5$. However, we show that the missing very soft X-ray emission could be absorbed by the cold gas in the filaments with an integrated hydrogen column density of $N_{\rm H} \sim 1.6 \times 10^{21}$ cm^{-2}, providing a natural explanation for the apparent temperature floor to the X-ray emission at $kT \sim 0.5$ keV. The internal reddening observed in the optical band indicates a similar level of intrinsic absorption.
6. The FIR through UV line emission is most likely primarily powered by the ICM particles penetrating the cold gas following a shearing induced mixing process. An additional source of energy may, in principle, be provided by X-ray photoionization from cooling X-ray emitting plasma.
7. The relatively small line ratio of [O I]/[C II] < 7.2 indicates a large optical depth in the FIR lines. The large optical depth at FIR and the intrinsic absorption inferred from the X-ray and optical data all imply significant reservoirs of cold atomic and molecular gas distributed in filaments with small volume filling fraction, but large area covering factor.

This work is based in part on observations made with *Herschel*, a European Space Agency Cornerstone Mission with significant participation by NASA. Support for this work was provided by NASA through award number 1428053 issued by JPL/Caltech. Support for this work was provided by NASA through Einstein Postdoctoral grant numbers PF9-00070 (A.S.) and PF2-130104 (R.v.W.) awarded by the Chandra X-ray Center, which is operated by the Smithsonian Astrophysical Observatory for NASA under contract NAS8-03060. S.W.A. acknowledges support from the U.S. Department of Energy under contract number DE-AC02-76SF00515. M.R. acknowledges NSF grant AST 1008454.

REFERENCES

Allen, S. W., Fabian, A. C., Edge, A. C., Bohringer, H., & White, D. A. 1995, MNRAS, 275, 741
Allen, S. W., Taylor, G. B., Nulsen, P. E. J., et al. 2001, MNRAS, 324, 842
Baldwin, J. A., Phillips, M. M., & Terlevich, R. 1981, PASP, 93, 5
Begelman, M. C., & Fabian, A. C. 1990, MNRAS, 244, 26P
Beiersdorfer, P., Schweikhard, L., Liebisch, P., & Brown, G. V. 2008, ApJ, 672, 726
Biretta, J. A., Sparks, W. B., & Macchetto, F. 1999, ApJ, 520, 621
Blakeslee, J. P., Jordán, A., Mei, S., et al. 2009, ApJ, 694, 556
Bohlin, R. C., Savage, B. D., & Drake, J. F. 1978, ApJ, 224, 132
Canning, R. E. A., Fabian, A. C., Johnstone, R. M., et al. 2011, MNRAS, 417, 3080
Churazov, E., Brüggen, M., Kaiser, C. R., Böhringer, H., & Forman, W. 2001, ApJ, 554, 261
Churazov, E., Forman, W., Vikhlinin, A., et al. 2008, MNRAS, 388, 1062
Cowie, L. L., & McKee, C. F. 1977, ApJ, 211, 135
Cravens, T. E. 1997, GeoRL, 24, 105
Crawford, C. S., Allen, S. W., Ebeling, H., Edge, A. C., & Fabian, A. C. 1999, MNRAS, 306, 857
Crawford, C. S., & Fabian, A. C. 1992, MNRAS, 259, 265
Crawford, M. K., Genzel, R., Townes, C. H., & Watson, D. M. 1985, ApJ, 291, 755
Dennerl, K. 2002, A&A, 394, 1119
Dennerl, K. 2010, SSRv, 157, 57
de Plaa, J., Werner, N., Simionescu, A., et al. 2010, A&A, 523, A81
Donahue, M., Mack, J., Voit, G. M., et al. 2000, ApJ, 545, 670
Donahue, M., Stocke, J. T., & Gioia, I. M. 1992, ApJ, 385, 49
Donahue, M., & Voit, G. M. 1991, ApJ, 381, 361
Edge, A. C. 2001, MNRAS, 328, 762
Edge, A. C., & Frayer, D. T. 2003, ApJL, 594, L13
Edge, A. C., Oonk, J. B. R., Mittal, R., et al. 2010, A&A, 518, L46
Esquivel, A., Benjamin, R. A., Lazarian, A., Cho, J., & Leitner, S. N. 2006, ApJ, 648, 1043
Fabian, A. C., Allen, S. W., Crawford, C. S., et al. 2002, MNRAS, 332, L50
Fabian, A. C., Johnstone, R. M., Sanders, J. S., et al. 2008, Natur, 454, 968

Fabian, A. C., Sanders, J. S., Williams, R. J. R., et al. 2011, MNRAS, 417, 172
Falcke, H., Rieke, M. J., Rieke, G. H., Simpson, C., & Wilson, A. S. 1998, ApJL, 494, L155
Feretti, L., Dallacasa, D., Govoni, F., et al. 1999, A&A, 344, 472
Ferland, G. J., Fabian, A. C., Hatch, N. A., et al. 2008, MNRAS, 386, L72
Ferland, G. J., Fabian, A. C., Hatch, N. A., et al. 2009, MNRAS, 392, 1475
Ford, H. C., & Butcher, H. 1979, ApJS, 41, 147
Forman, W., Nulsen, P., Heinz, S., et al. 2005, ApJ, 635, 894
Friedman, S. H., Heinz, S., & Churazov, E. 2012, ApJ, 746, 112
Fujimoto, R., Mitsuda, K., Mccammon, D., et al. 2007, PASJ, 59, 133
Gaspari, M., Ruszkowski, M., & Sharma, P. 2012, ApJ, 746, 94
Gladstone, G. R., Waite, J. H., Grodent, D., et al. 2002, Natur, 415, 1000
Grevesse, N., & Sauval, A. J. 1998, SSRv, 85, 161
Hatch, N. A., Crawford, C. S., Fabian, A. C., & Johnstone, R. M. 2005, MNRAS, 358, 765
Hatch, N. A., Crawford, C. S., Johnstone, R. M., & Fabian, A. C. 2006, MNRAS, 367, 433
Heckman, T. M. 1980, A&A, 87, 152
Heckman, T. M., Baum, S. A., van Breugel, W. J. M., & McCarthy, P. 1989, ApJ, 338, 48
Hines, D. C., Eilek, J. A., & Owen, F. N. 1989, ApJ, 347, 713
Jaffe, W., & Bremer, M. N. 1997, MNRAS, 284, L1
Jaffe, W., Bremer, M. N., & Baker, K. 2005, MNRAS, 360, 748
Jaffe, W., Bremer, M. N., & van der Werf, P. P. 2001, MNRAS, 324, 443
Johnstone, R. M., Fabian, A. C., & Nulsen, P. E. J. 1987, MNRAS, 224, 75
Johnstone, R. M., Hatch, N. A., Ferland, G. J., et al. 2007, MNRAS, 382, 1246
Kaastra, J. S., Mewe, R., & Nieuwenhuijzen, H. 1996, in UV and X-Ray Spectroscopy of Astrophysical and Laboratory Plasmas, ed. K. Yamashita & T. Watanabe (Tokyo: Universal Academy Press), 411
Kalberla, P. M. W., Burton, W. B., Hartmann, D., et al. 2005, A&A, 440, 775
Kaufman, M. J., Wolfire, M. G., Hollenbach, D. J., & Luhman, M. L. 1999, ApJ, 527, 795
Kewley, L. J., Groves, B., Kauffmann, G., & Heckman, T. 2006, MNRAS, 372, 961
Lazarian, A., Kowal, G., Vishniac, E., & de Gouveia Dal Pino, E. 2011, P&SS, 59, 537
Lazarian, A., Santos-Lima, R., & de Gouveia Dal Pino, E. 2010, in ASP Conf. Ser. 429, Numerical Modeling of Space Plasma Flows, Astronum-2009, ed. N. V. Pogorelov, E. Audit, & G. P. Zank (San Francisco, CA: ASP), 113
Lisse, C. M., Dennerl, K., Englhauser, J., et al. 1996, Sci, 274, 205
Liu, J., Mao, S., & Wang, Q. D. 2011, MNRAS, 415, L64
Liu, J., Wang, Q. D., & Mao, S. 2012, MNRAS, 420, 3389
Malhotra, S., Helou, G., Stacey, G., et al. 1997, ApJL, 491, L27
Malhotra, S., Kaufman, M. J., Hollenbach, D., et al. 2001, ApJ, 561, 766
McCourt, M., Sharma, P., Quataert, E., & Parrish, I. J. 2012, MNRAS, 419, 3319
McDonald, M., Veilleux, S., Rupke, D. S. N., & Mushotzky, R. 2010, ApJ, 721, 1262
McDonald, M., Wei, L. H., & Veilleux, S. 2012, ApJL, 755, L24
Million, E. T., Werner, N., Simionescu, A., et al. 2010, MNRAS, 407, 2046
Mittal, R., O'Dea, C. P., Ferland, G., et al. 2011, MNRAS, 418, 2386
Mittal, R., Oonk, J. B. R., Ferland, G. J., et al. 2012, MNRAS, 426, 2957
O'Dea, C. P., Baum, S. A., Privon, G., et al. 2008, ApJ, 681, 1035
Oonk, J. B. R. 2011, PhD thesis, Univ. Leiden
Oonk, J. B. R., Jaffe, W., Bremer, M. N., & van Weeren, R. J. 2010, MNRAS, 405, 898
Osterbrock, D. E., & Ferland, G. J. 2006, Astrophysics of Gaseous Nebulae and Active Galactic Nuclei (Sausalito, CA: University Science Books)
Pilbratt, G. L., Riedinger, J. R., Passvogel, T., et al. 2010, A&A, 518, L1
Poglitsch, A., Waelkens, C., Geis, N., et al. 2010, A&A, 518, L2
Revaz, Y., Combes, F., & Salomé, P. 2008, A&A, 477, L33
Robertson, I. P., Cravens, T. E., Snowden, S., & Linde, T. 2001, SSRv, 97, 401
Salomé, P., & Combes, F. 2003, A&A, 412, 657
Salomé, P., & Combes, F. 2008, A&A, 489, 101
Salomé, P., Combes, F., Edge, A. C., et al. 2006, A&A, 454, 437
Salomé, P., Combes, F., Revaz, Y., et al. 2011, A&A, 531, A85
Salomé, P., Revaz, Y., Combes, F., et al. 2008, A&A, 483, 793
Sanders, J. S. 2006, MNRAS, 371, 829
Sanders, J. S., & Fabian, A. C. 2007, MNRAS, 381, 1381
Sanders, J. S., & Fabian, A. C. 2011, MNRAS, 412, L35
Sanders, J. S., Fabian, A. C., Allen, S. W., et al. 2008, MNRAS, 385, 1186
Sanders, J. S., Fabian, A. C., Frank, K. A., Peterson, J. R., & Russell, H. R. 2010, MNRAS, 402, 127
Sanders, J. S., Fabian, A. C., & Taylor, G. B. 2009, MNRAS, 396, 1449
Sharma, P., McCourt, M., Quataert, E., & Parrish, I. J. 2012, MNRAS, 420, 3174
Simionescu, A., Werner, N., Finoguenov, A., Böhringer, H., & Brüggen, M. 2008, A&A, 482, 97
Sparks, W. B., Donahue, M., Jordán, A., Ferrarese, L., & Côté, P. 2004, ApJ, 607, 294
Sparks, W. B., Ford, H. C., & Kinney, A. L. 1993, ApJ, 413, 531
Sparks, W. B., Pringle, J. E., Carswell, R. F., et al. 2012, ApJL, 750, L5
Sparks, W. B., Pringle, J. E., Donahue, M., et al. 2009, ApJL, 704, L20
Stacey, G. J., Geis, N., Genzel, R., et al. 1991, ApJ, 373, 423
Taylor, G. B., Fabian, A. C., Gentile, G., et al. 2007, MNRAS, 382, 67
Taylor, G. B., Govoni, F., Allen, S. W., & Fabian, A. C. 2001, MNRAS, 326, 2
Wargelin, B. J., Markevitch, M., Juda, M., et al. 2004, ApJ, 607, 596
Werner, N., Böhringer, H., Kaastra, J. S., et al. 2006, A&A, 459, 353
Werner, N., Simionescu, A., Million, E. T., et al. 2010, MNRAS, 407, 2063
Werner, N., Sun, M., Bagchi, J., et al. 2011, MNRAS, 415, 3369
Young, A. J., Wilson, A. S., & Mundell, C. G. 2002, ApJ, 579, 560